RADII AND EFFECTIVE TEMPERATURES FOR G, K AND M GIANTS AND SUPERGIANTS

G.T. VAN BELLE, B.F. LANE
Jet Propulsion Laboratory, California Institute of Technology, 4800 Oak Grove Dr., MS 306-388, Pasadena, CA 91109

R.R. THOMPSON
Department of Physics and Astronomy, University of Wyoming, Laramie, Wyoming 82071

A.F. BODEN, M.M. COLAVITA, D.W. MOBLEY, D. PALMER, M. SHAO, J.K. WALLACE
Jet Propulsion Laboratory, California Institute of Technology, 4800 Oak Grove Dr., MS 306-388, Pasadena, CA 91109

M.J. CREECH-EAKMAN, C.D. KORESKO, S.R. KULKARNI, X.P. PAN
California Institute of Technology, 4800 Oak Grove Dr., MS 306-388, Pasadena, CA 91109

J. GUBLER
UC San Diego

ABSTRACT

Interferometrically determined angular diameters obtained at the Palomar Testbed Interferometer (PTI) for 80 giant and supergiant stars are presented in this paper. Spectral types of the 69 giant stars lie generally between G6 and M6, though there is a B7 giant diameter reported herein as well; the 9 bright giants and supergiants have spectral types between F5 and M5. Comparison of the results to those from the IOTA interferometer indicate no statistically significant difference between the two datasets. In conjunction with the previous results as reported by Dyck *et al.* (1996, 1998), the 123 giant stars provide empirically determined dependencies of effective temperature and linear radius upon spectral type and V-K color.

1. Introduction

Interferometric observations of giant and supergiant stars have begun to be reported in the literature with an increasing frequency as interferometric telescopes come online and mature. Observers at installations such as IOTA (the IR Optical Telescope Array), NPOI (the Navy Prototype Optical Interferometer) and PTI (the Palomar Testbed Interferometer) have been utilizing their capability to resolve stars in the <20 milliarcsecond (mas) range to produce a large body of results on evolved stars. These results are significant in that constitute direct measurement of the parameters of stars that populate the coolest, most luminous portion of the HR diagram. Efforts over the past year to characterize and utilize PTI have resulted in a large body of data being produced on the subject by PTI. In this paper we report new visibility observations for 80 evolved stars obtained at PTI. The recent release of the Hipparcos results (Perryman *et al.* 1997) has had the added benefit of allowing many of the observed angular sizes to be interpreted as linear radii as well. Together with the previous angular size results obtained at IOTA by our group as reported in Dyck *et al.* (1996, 1998, henceforth Papers I and II, respectively), we have been able to empirically characterize the effective temperature and linear radii as a function of spectral type and a variety of colors.

2. Observations

2.1 The Interferometer

PTI is a three-aperture interferometer located atop Palomar Mountain in San Diego County, CA. Two of the 40 cm apertures may be used in conjunction for any single interferometric observation. The north and south piers used in this investigation are 110m apart on a baseline 11º east of true north; the west pier (now operational, but not used for this paper) is located approximately 85m from the first two piers. Light from the two telescopes being linked interferometrically is reflected by transport optics into a central beam combining laboratory, where two delay lines are located. One of the two delay lines operates as a 'move-and-hold' element in the beam train for one of the telescopes, while the second moves dynamically during an observation with a precision of 10 nm. Following the delay line elements, the starlight is directed onto a recombination table, where dichroics split off the visible light for tip-tilt tracking by 4 fiber-fed avalanche photodiodes. After the dichroics, the two telescope beams are recombined at a beam splitter. One of the two outputs from the beam splitter is fed directly into a dewar onto a single pixel of a NICMOS3 detector; this signal is referred to as the 'white-light channel'. The other output is fed through a single-

mode fiber and a prism outside the dewar, then onto seven pixels on the detector chip; this signal constitutes the 'spectrometer channels'. Effective integration time for each pixel is 6.75 ms. The white-light channel was utilized for fringe tracking in a manner similar to that use at the Mark III interferometer as described in Shao *et al.* (1988).

The channels used for visibility amplitude measurements reported herein were the spectrometer channels, which range in seven 0.07 μm bins across the K band centered at 1.99, 2.06, 2.13, 2.20, 2.27, 2.34, and 2.41 μm. (A new experimental setup for the 1998 observing season onward will have 5, not 7, spectral channels.) These channels, having been routed through a single-mode fiber before detection, were considerably less noisy than the white-light channel. Due to low flux levels, the two edge spectrometer pixels were dropped; the resulting 5 pixels were averaged, resulting in an effective white-light K band measurement, of wavelength λ=2.19±0.01 μm. For a more complete description of the instrument, see Colavita *et al.* (1998).

2.2 Data Reduction

Post-processing of the fringe data provides measurements of fringe amplitude in 25 second bins; typically each observation of a star, calibrator or science target, will contain four or five of these bins. These raw V^2s then are then normalized by comparison of the science target V^2s to calibrator object V^2s. The primary calibrator objects were main sequence stars which are expected to be nearly unresolved by the interferometer (less than 0.70 mas). Given that even these objects would have their disks marginally resolved, the observed calibrator V^2s were increased slightly for expected angular size. These adjustments were less than 5%, however, since a 0.70 mas object would have a V^2 of roughly 0.95. Expected angular size was based upon radius from spectral type (Allen 1973) and distance (Perryman 1997); an error bar of 20% was assumed for the radius. The primary calibrators are listed in Table 1. We note that one of our primary calibrators is 51 Peg; despite its noted radial velocity variability, an extensive interferometric campaign to detect V^2 variations has indicated this object is stable at a level of ΔV^2=1.5% (Boden *et al.* 1998).

Secondary calibrator objects were giant stars that were also expected to be nearly unresolved by the interferometer (less than 0.90 mas), but less so than the primary calibrators; a 0.90 mas object has an expected V^2 of 0.90. Angular sizes of these objects were estimated from spectral types and distances, *but verified* based upon nearby primary calibrator objects. The purpose of secondary calibrators was to allow science targets to be selected from around the sky even if a primary calibrator was not within 15º; secondary calibrators allow for extension of sky coverage with nearby calibrators, albeit with lower accuracy as the error bars propagate.

Science objects that had more than one calibrator nearby in time (±1 hour) and space (0-15º) utilized all calibration visibilities in a weighted sense, based upon locality and statistical weight. For those objects with 2 or more calibrators, separate normalizations were calculated and compared for consistency. In this fashion both the system performance as characterized by the calibrator visibility, and adjustments to calibrator visibility were established as consistent. Roughly 80% of the science targets observed had at least two nearby calibration objects observed contemporaneously; half of those had three or more calibration objects nearby.

Assuming a uniformly irradiating disk, once a normalized value for V^2 has been obtained, an angular size can be obtained by fitting $V^2=(2J_1(x)/x)^2$, where $x=\theta_{UD}\pi D/\lambda$. Given the expected departures from a uniform disk (primarily the presence of limb darkening), this assumption is not exactly accurate. We will adjust for that in §3, noting that expected departures will be small (cf. Paper II, Tuthill 1994). Since the uniform disk function repeats at low visibility levels, care must be taken to utilize only the monotonic region of the function, found at spatial frequencies for which V^2>0.017; for the 110m baseline of PTI, this corresponds to θ_{UD}=4.34 mas.

2.3 Target Selection

Target selection was accomplished by collecting as large a sample of potential targets as possible. First, The Catalog of Infrared Observations (Gezari 1996) was scanned for all measurements with m_K<5 in the proper declination range (0º < δ < 55º). A cross-correlation of the resultant list with the SIMBAD database then allowed for a further cut for those objects with m_V<7, due to limitations in the star acquisition system at the time of the observations. The general object types as reported by SIMBAD and spectral types were used to obtain yet a further cut of those objected reasonably expected to be luminosity class I, II or III stellar objects. Angular sizes were then estimated based upon one of two methods: either 1) selection as above for calibrators, where spectral types were used in estimating linear radius, and combined with Hipparcos distances to obtain angular size; or 2) photometry as reported by SIMBAD was utilized in estimating bolometric flux, and then combined with effective temperatures as expected by spectral type to obtain an angular size estimate. Those objects that met the requirement for resolvability by PTI (1.8 mas < θ_{EST} < 4.3 mas, where a 1.8 mas object will have V^2 ~ 0.80 for PTI) were then eligible for the

observing list. Given the constraints of available observing time for this observing season and the large number of potential science targets, objects that crossed the meridian 10º to either side of the zenith ($21º < \delta < 41º$) were given priority in the observing queue to minimize observing airmass. Given the more than adequate results from the interferometer observing these objects at large hour angles (HA > 2), this appears to have been an arbitrary limitation on the source list and will be discontinued in the future.

2.4 Night-to-night Repeatability

Utilizing nightly weighted average values for normalized V^2, the average standard deviation from night-to-night was found to be $\Delta V^2=0.018$ for stars that were observed on at least three nights. This represents a variety of seeing conditions and calibration sources for the stars. The primary limitation appears to be the degree to which angular sizes of calibration sources can be determined, based upon known spectral types and photometric information for these sources. By way of comparison, the experimental setup utilized at the IOTA interferometer provided a night-to-night measurement accuracy of roughly $\Delta V^2=0.051$ (Paper I). The reason for this improvement in normalized visibility is due in part to the use of a single-mode fiber in the PTI beam train; a related experimental setup of the IOTA facility produced comparable results (Perrin *et al.* 1995).

2.5 Comparison to Previous Results

Unfortunately, there are few results in the literature with which to compare to the results from PTI. We will compare general results (e.g., spectral type vs. effective temperature) in §3; however, there are only seven specific examples of stars with angular sizes in both the literature and in our dataset. Of these, four are inferred diameters from the infrared flux method (IRFM, see Blackwell *et al.* 1979); three are measurements from occultations and interferometry. These data points are listed in Table 2.

The dearth of comparative datapoints has a twofold explanation. First, interferometrically determined diameters available in the literature are few in number. Second, aggravating the problem presented by the limited data generally available, PTI's stellar disk angular resolution is slightly finer than previously available to interferometry (in the 1-4 mas range, as opposed to the 4+ mas range). Hence, the stars examined with PTI are slightly smaller in physical size, which in turn translates to stars of a slightly earlier spectral type than observed with other interferometers, such as IOTA, IRMA, CERGA and the Mark III. Some stars of later spectral type (M0 on) were observed with PTI, but this is a function of its greater infrared sensitivity (roughly two magnitudes better at K than the experimental setup at IOTA utilized in Papers I and II).

The IRFM sizes and temperatures are in good agreement with the PTI data. The temperatures are, on average, less than one sigma away from those measured with PTI; the angular sizes are between 2 and 3 sigma away from those determined by PTI, but still in quite comparable to the IRFM numbers. The one occultation value, for HR 2630, is consistent with the upper bound from Richichi *et al.* (1996). The previous interferometric results, however, bear some close examination.

For HR 1791, the value of 1.15±0.05 mas appears to be in contradiction to the PTI value of 1.50±0.16 mas. However, upon closer examination, Mozurkewich *et al.* (1991) states that the systematic errors could potentially be considerably larger than the formal errors quoted in the paper. Furthermore, the angular size for this object, obtained with the Mark III interferometer, does not appear to have been directly obtained from interferometric data but adopted indirectly from surface brightness assumptions. For HR 8684, the value of 4.9±0.4 mas given by Hutter *et al.* (1989) is strikingly different from our measurement of 2.62±0.09 mas. However, we simply point out that, given the bolometric flux of this object, the larger angular size implies an effective temperature of ~3600 K. This is roughly 1100 K cooler for the temperature expected for a G8III star (TBD), which is the well-determined spectral type for the star (Morgan & Keenan 1973). We submit that the previously reported angular size is erroneous. Furthermore, the temperature that is obtained from PTI data (~5000 K) is consistent both with the spectral class and with the value predicted from IRFM (Castelli *et al.* 1997).

3. The Data

3.1 Additional sources of data

In order to properly estimate bolometric fluxes for the stars observed, broadband photometry was needed to sample that flux, particularly in the near- to mid-IR where these stars emit much of their light. Magnitudes at 2.2 μm for the stars observed were found in Gezari *et al.* (1996). The 12 μm fluxes available for our targets from the IRAS Point Source Catalog (1987) were used as magnitudes, as described in Hickman *et al.* (1995):

$[12] = -2.5 \log (f_{12\mu m} / 28.3 \text{ Jy})$

Reddening corrections based upon the empirical reddening determination described by Mathis (1980). As discussed in Paper I, this determination differs little from van de Hulst's theoretical reddening curve number 15 (see Johnson 1968). The effects of reddening are, at worst, minimal, given the majority of bolometric flux contribution coming from relatively unaffected bandpasses, and given the proximity of the majority of the objects observed (< 200 pc) – at 2.2 μm, a source at 200 pc will typically have A_K=0.04. Monochromatic flux densities at each wavelength were obtained from the magnitudes using absolute calibrations by Hayes & Latham (1975), Hayes (1984) and Blackwell *et al.* (1983). Bolometric flux densities were generally computed from a simple numerical integration of the observed monochromatic flux densities from 0.45 to 12 μm, as found in the SIMBAD database. Flux contributions beyond 12 μm were estimated by integrating a Rayleigh-Jeans distribution, normalized to the 12 μm flux density. Errors in the bolometric flux were estimated directly from the contribution of the photometric errors for each data point for a given star; average error in the determination of the bolometric flux was 18%. This compares favorably with the similar technique employed in Papers I and II, where the F_{TOT} error was merely assumed to be 15% for all stars.

We have been careful to choose stars that are classified on the MK system, preferring spectral types estimated by Morgan or Keenan and their coworkers. Second choices have been spectral types from Hoffleit (1982) and Eggen (1967, 1976, 1992), which correlate very well with the Keenan types. In some cases, alternative sources were necessary; references in Table 5 indicate the origin of each star's spectral typing.

Lastly, angular size data available in Papers I and II has been utilized in this manuscript, for two specific reasons. First, the data represent an independent body of interferometric data, taken at a separate instrument and processed with different data reduction software. The consistency of the results between the two interferometers is evidence for the soundness of the technique employed in this paper, as well as Papers I and II. Second, the sample size as increased by data not only from PTI but also from IOTA allows us to extend the generalization of our results over a range of spectral classes and colors.

3.2 Temperature and Radius

In deriving values for temperature and radius from the PTI observations, it is important to keep in mind that these quantities derive from angular sizes measured in the K band. This particular bandpass offers a number of advantages. First, it is well known that many stars - particularly those of the latest spectral types - exhibit evidence of circumstellar dust shells. This dust can be difficult to separate from the photosphere, making photospheric diameter determinations difficult, as pointed out by Tsuji (1978). The near-infrared avoids both the scatter of optical wavelengths and the thermal reradiation at longer infrared bandpasses, penetrating to the stellar photosphere. Second, as discussed below, the effects of limb darkening in the near-infrared are minimized relative to shorter wavelengths. Third, angular sizes at these wavelengths are easily compared to those measured in previous investigations of this nature.

Stellar effective temperature, T_{EFF}, is defined in terms of the star's luminosity and radius by $L=4\pi\sigma R^2 T_{EFF}^4$. Rewriting this equation in terms of angular diameter θ_R and bolometric flux F_{TOT}, T_{EFF} can be expressed as $T_{EFF}=2341(F_{TOT}/\theta_R^2)^{1/4}$; the units of F_{TOT} are 10^{-8} erg cm^{-2} s^{-1}, and θ_R is in mas. The angular size utilized here is the Rosseland angular diameter, which corresponds to the surface where the Rosseland mean optical depth equals unity. As advocated by Scholz & Takeda (1987), this is the most appropriate surface for computing an effective temperature; utilizing the same evaluation of Scholz & Takeda's model atmospheres found in Papers I and II, we calculate the relationship $\theta_R \approx 1.022\ \theta_{UD}$ in the K band. Thus, in the infrared this effect is well contained within the errors of this investigation, but is included for completeness. The effect is not as marginal in other wavelength bands (see van Belle *et al.* 1996 for a discussion).

Stellar radius is given by $R=0.1076\ \theta_R/d$; the units of R are R_{SUN}, d is in parsecs, and θ_R is again the Rosseland diameter. Distances were obtained from the parallaxes of Hipparcos (Perryman *et al.* 1997); distances (and associated radii) with errors in excess of 20% were discarded.

4. Empirical Relationships for Giant Stars

4.1 Spectral Type

The effective temperature scale as a function of spectral type of K and M giants is a topic that has already been well-studied (Ridgway *et al.* 1980, DiBenedetto & Rabbia 1987, Paper I, II). As a check of the veracity of our results, it is worthwhile to compare the effective temperature scale obtained in this study to that of Paper II. The fit from Paper II is T_{EFF}=-106×ST + 4580 K, where ST=-2,...0,...5,6,...8 corresponding to spectral classes G8,...,K0,...,K5,M0,...,M8.

Comparing the PTI data to this fit, we find that average absolute difference to be 140 K, and the average difference is less than 20 K; comparing the average absolute difference to the RMS spread of each bin, we find that the mean is less than half of a standard deviation for the PTI data, which is good agreement.

A fit of the composite dataset gives: T_{EFF} = -105 × ST + 4530 K, with a reduced χ^2 of 4.21. This fit is statistically identical to the one given in Paper II, although it is marginally hotter for both the earlier spectral types (~60 K for G8III) and the later spectral types (~40 K for M7III). It is reasonable to expect that this is due to either a slight bias in either the IOTA sample to cooler, larger stars, or conversely, one in the PTI sample towards hotter, smaller stars. By spectral type bin, the average standard deviation of the temperatures is $\Delta T_{rms} \approx 270$K.

Given the large dataset for the giant stars and the recent release of the Hipparcos data (1997), we also draw some general conclusions about the dependence of linear radii upon spectral subtype. A weighted exponential fit to the data results in the following relationship: R=3.2 + 10.6×$10^{0.094 \times ST}$ R_{SUN}, with a reduced χ^2 of 9.49 (noting that an *linear* fit to the data results in a reduced χ^2 of 17.8). The poor χ^2 is a shortcoming of the fit due to the scaling of error bars with star size due to the primary error source being parallactic error; as such, the earlier spectral types are potentially better fit, at the expense of the later spectral type.

Given the poor χ^2, a better predictor of radius as a function of spectral type is actually average values by spectral type bin, which is not affected by the scaling of radius errors for the larger stars. The sizes predicted by the bins tend to be slightly (~35%) larger than comparable numbers expected from Paper I. This is consistent with the result that the space-based Hipparcos parallax numbers tended to indicate distances greater than expected from ground-based parallaxes, which were all that were available at the time of Paper I's writing. However, we are in agreement with observation from Paper I that a factor of 2 increase in size accompanies every 500 K decrease in effective temperature. Examining the means and standard deviations by spectral type bin, we see that on average the standard deviations are 60% of the mean values, indicating the limitations of spectral-type inferred sizes. A more robust inference is derived from V-K color (§4.2). Comparing to sizes as estimated from Dumm & Schild (1998), the mean size by spectral type bin agrees quite well; on average, our sizes are 98% of the sizes given by Dumm & Schild. The spectral type-dependent data and resultant fits may be seen in Figures 1a and 1b, and Table 7.

4.2 V-K Color, K-[12] Color

Given the potential of misclassifications even when being selective about sources of spectral typing, a second parameter used in investigating the potential dependencies of stellar temperature and size was giant star color, as characterized by both V-K and K-[12]. An interesting additional comparison that can be drawn for both of these colors is the departure of the observed stars' temperatures from nominal blackbody behavior, as blackbody temperatures can be well-determined from the Planck function for any given value of V-K or K-[12].

V-K Color. A numerical comparison of the agreement of the IOTA and PTI datasets was not readily possible using fits given the rather separate sample space of the two datasets ($2 < V\text{-}K_{PTI} < 5$, while $3 < V\text{-}K_{IOTA} < 9$) and the exponential nature of the empirical function. However, by inspection, the region of overlap was in good agreement, and the resultant fit to the composite data set greatly benefited from the wide coverage of the data points. The exact form is: T = 2980 + 4085×$10^{-0.377 \times (V-K)}$ K, with a reduced χ^2 of 2.74. A plot of the data, the fit, and the corresponding black-body curve can be seen in Figure 2a. In Table 8, binned averages and fits for the temperature data are presented for bins ranging from 2.0 to 9.0, in addition to the corresponding numbers for the radius data. One of the most striking features of Figure 2a is the departure of the temperature data points from expected blackbody behavior. This is reflected in Table 8, where all of the mean temperatures deviate from blackbody temperatures by 3σ or more for V-K ≥ 6.0.

A similar exercise exploring the radius data as a function of V-K color delivers the following function: R = -34.2 + 22.6×$10^{0.135 \times (V-K)}$ R_{SUN}, with a reduced χ^2 of 9.88. As with the radius-spectral type fit, this particular function

has a poor χ^2, and the mean radius values seen in the V-K bins are a better indicator of the expected relationship between V-K and radius. Examining the means and standard deviations by spectral type bin, we see that on average the standard deviations are 35% of the mean values. A plot of the stellar radii as a function of V-K can be seen in Figure 2b.

An exclusion from both of the V-K fits is BS 274. This particular object has an unusually low temperature and large size for both its spectral classification (G6III) and V-K color (2.49). Given that this particular object was observed on only one night, the possibility exists for either an anomalous measurement or a unexpected secondary companion; further observations of this object during the upcoming observing season are expected to resolve the source of the anomaly.

K-[12] Color. Neither linear nor exponential fits of temperature or radius as a function of K-[12] color were statistically significant. However, as with the behavior seen for the V-K data, one of the most striking features of the temperature versus K-[12] plot is the departure of the temperature data points from expected blackbody behavior. This is reflected in Table 9, where all of the mean temperatures deviate from blackbody temperatures by 2.5σ or more for K-[12] ≥ 0.80. A general trend of stellar radii towards larger values (R>100 R_{SUN}) are seen for K-[12] ≥ 0.80 as well. Both the temperature and radius plots can be seen in Figures 3a and 3b; temperature averages and standard deviations are listed in the table for bins from 0.35 < K-[12] < 1.80.

An exclusion from both of the K-[12] fits is BS 7995. This particular object has a temperature and radius consistent with its spectral classification (G7III), although it appears to have an anomalously red K-[12] color (0.80). Unlike BS 274 (see above), this object was object was observed on multiple nights, and there appears little room for questioning the angular size; we believe that our value obtained for the K-[12] is the more likely source of error.

Departures from Blackbody Behavior. Both the V-K and K-[12] data deviate from blackbody behavior at a stellar effective temperature of T≈3500K; the shorter wavelength color shows a gradual departure from the BBR curve, while the longer wavelength color indicates a sharper turn-off. Several mechanisms are being explored as reasonable explanations for the deviation from the blackbody curves. Equivalent widths of absorption features in the K band, particularly ^{12}CO(2,0) at 2.29 μm, grow with decreasing temperature (Ramirez *et al.* 1997). However, there does not appear to be any sharp onset of this effect at 3500K; indeed, the gradual appearance of this and other K band absorption features begins at a much warmer temperature of 4600K. Preliminary inspection of the visibilities from individual spectral channels available from PTI also show no evidence for specific features at the narrow bandpass channel that contains the ^{12}CO(2,0) feature. V band absorption features, such as Mg_1, Mg_2 and TiO, appear as likely candidates in depressing V relative to K for low temperatures (Barbuy *et al.* 1992, Jørgensen 1994). K-[12] color is a reasonable indicator of mild dusty mass loss (Le Sidander & Le Bertre 1996), and the 12 μm excesses are quite consistent with rates between 10^{-10} M_{SUN} yr^{-1} (Le Sidander & Le Bertre) and $10^{-7} - 10^{-8}$ M_{SUN} yr^{-1} (Beichman *et al.* 1990); scattering of short-wavelength light by a dusty envelope would also produce the V-K excess.

5. Bright Giants and Supergiants

As we previously observed in Paper II, a plot of the radius versus temperature for the luminosity class I, II and III objects exhibited a tendency for the higher luminosity objects to have a greater radius at a given temperature. On average, the luminosity class I and II objects were ~3 times larger than their giant star counterparts at a given temperature. A plot of the total data set for giants and supergiants can be seen in Figure 4.

Again, as with Paper II, the limitations in the available distance data are what preclude the construction of an HR diagram from the data on hand. While the release of the Hipparcos data has greatly enabled the investigations into radius of this paper, the limitations of the data still restrict the derivable luminosities.

6. Conclusion

Further parameterization of the fits to the stars in our observed sample has the potential to greatly reduce the spread in those fits, particularly those as a function of V-K color. Specifically, characterization of surface gravity g in a manner independent of assumptions about a star's mass M can lead to determinations of M from g and linear radius. Preliminary research into this line of thinking appears to be quite promising and will be the subject of a forthcoming manuscript. Continuing observations at PTI will increase the size of our available database, and will specifically concentrate upon luminosity class I and II objects, in addition to giant stars with spectral types earlier than G7.

Acknowledgments. This research has made use of the SIMBAD and VizieR databases, operated by the CDS, Strasbourg, France. We gratefully thank the staffs of the Palomar Observatory and Whipple Observatory for

their hospitality during our many stays. GTvB and BT were supported while students at the University of Wyoming by a grant from the PASS Center, and would like to acknowledge Ron Canterna for use of computer resources at UW. HMD acknowledges support from NSF grant AST-958129 while he was at the University of Wyoming. Portions of this work were performed at the Jet Propulsion Laboratory, California Institute of Technology under contract with the National Aeronautics and Space Administration.

References

Allen, C.W., 1973, Astrophysical Quantities, (Athlone Press, London).
Barbuy, B., Erdelyi-Mendes, M., Milone, A., 1992, *A&AS*, **93**, 235.
Beichman, C. A., Chester, T., Gillett, F. C., Low, F. J., Matthews, K., Neugebauer, G., 1990, *AJ*, **99**, 1569.
Bidelman, W.P., 1957, *PASP*, **69**, 147.
Blackwell, D.E., Shallis, M.J., Selby, M.J., 1979, *MNRAS*, **188**, 847.
Blackwell, D. E. *et al.* 1983, *MNRAS*, **205**, 897
Blackwell, D.E. & Lynas-Gray AE 1994, *A&A*, **282**, 899.
A. Boden, G. van Belle, M. Colavita, J. Gubler, C. Koresko, S. Kulkarni, B. Lane,D. Mobley, X. Pan, M. Shao, K. Wallace, 1998, *ApJL*, in press.
Castelli, F., Gratton, R.G., Kurucz, R.L., 1997, *A&A*, **318**, 841.
Colavita, M.M., *et al.* 1998, in preparation.
Cowley, A. 1972, *AJ*, **77**, 750.
DiBenedetto, G.P., Rabbia, Y., 1987, *A&A*, **188**, 114.
Dumm, T. & Schild, H., 1998, *New Astronomy*, in press.
Dyck, H.M., Benson, J.A., van Belle, G.T., Ridgway, S.T., 1996, *AJ* **111** 1705.
Dyck, H.M., van Belle, G.T., Thompson, R.R., 1998, submitted to *AJ*.
Eggen, O.J., 1967, *ApJS*, **14**, 307.
Eggen, O.J., 1976, *PASP*, **88**, 426.
Eggen, O.J., 1992, *AJ*, **104**, 275.
Fernie, J.D., 1983, *ApJS*, **52**, 7.
Gezari, D.Y., Pitts, P.S., Schmitz, M., Mead, J.M., Catalog of Infrared Observations, Edition 3.5, 1996 (Unpublished, available from VizieR).
Griffin, R.F., Redman, R.O., 1960, *MNRAS*, **120**, 287.
Haggkvist, L., Oja, T., 1987, *A&AS*, **68**, 259.
Hayes, D. S. 1984, Calibration of Fundamental Stellar Quantities, edited by D. S. Hayes, L. E. Pasinetti and A. G. D. Philip (Reidel, Dordrecht), p. 246
Hayes, D.S. & Latham, D.W. 1975, *ApJ*, **197**, 593
Heard, J.F., 1956, *Publ. David Dunlap Obs.*, **2**, 105.
Hickman, M.A., Sloan, G.C., Canterna, R.C., *AJ* **110** 2910.
Hutter, D. J., Johnston, K. J., Mozurkewich, D., Simon, R. S., Colavita, M. M., Pan, X. P., Shao, M., Hines, B. E., Staelin, D. H., Hershey, J. L., Hughes, J. A., Kaplan, G.H., 1989, *ApJ*, **340**, 1103.
IRAS Catalog of Point Sources, Version 2.0, 1987, (GPO & Greenbelt: NASA Astronomical Data Center, Washington, D.C.)
Jaschek, C., Conde, H., De Sierra, A.C., 1964, Catalogue Of Stellar Spectra Classified In The Morgan-Keenan System, [La Plata] : Observatorio Astronomico de la Universidad Nacional de la Plata.
Johnson, H. L. 1968, Nebulae and Interstellar Matter, edited by B. M. Middlehurst & L. H. Aller (University of Chicago Press, Chicago), chapter 5.
Jørgensen, U.G., 1994, *A&A*, **284**, 179.
Keenan, P.C., Keller, G., 1953, *ApJ*, **117**, 241.
Keenan, P.C., McNeil, R.C., 1989, *ApJS*, **71**, 245.
Le Sidaner, P., Le Bertre, T., 1996, *A&A*, **314**, 896.
Mathis, J. S. 1980, *ARAA*, **28**, 37
McWilliam, A. 1990, *ApJS*, **74**, 1075.
Metreveli, M.D., 1968, *Byull. Abastumanskaya Astrofiz. Obs.*, **38**, 93.
Moore & Paddock 1950, *ApJ*, **112**, 48.
Morgan, W.W., Keenan, P.C., 1973, *ARAA* **11** 29.

Morgan, W.W., Roman, N.G. 1950, *ApJ*, **112**, 362.
Mozurkewich, D., Johnston, K. J., Simon, Richard S., Bowers, P. F., Gaume, Ralph, Hutter, D. J., Colavita, M. M., Shao, M., Pan, X. P. 1991, *AJ*, **101**, 2207.
Noguchi, K., 1990, *PASJ*, **42**, 419.
Perrin, G., Coude Du Foresto, V., Ridgway, S.T., Mariotti, J.-M., Benson, J.A., 1995, *SPIE* **2476** 120.
Perryman, M. A. C., Lindegren, L., Kovalevsky, J., Hog, E., Bastian, U., Bernacca, P. L., Creze, M., Donati, F., Grenon, M., Grewing, M., Van Leeuwen, F., Van Der Marel, H., Mignard, F., Murray, C. A., Le Poole, R. S., Schrijver, H., Turon, C., Arenou, F., Froeschle, M., Petersen, C. S., 1997, *A&A*, **323**, L49.
Ramirez, S. V., Depoy, D. L., Frogel, J. A., Sellgren, K., Blum, R. D, 1997, *AJ*, **113**, 1411.
Richichi, A., Baffa, C., Calamai, G., Lisi, F.,1996, *AJ*, **112**, 2786.
Ridgway, S. T., Jacoby, G. H., Joyce, R. R., Wells, D. C., 1980, *AJ*, **85**, 1496.
Roman, N.G., 1952, *ApJ*, **116**, 122.
Sato, K., Kuji, S., 1990, *A&AS*, **85**, 1069.
Scholz, M., Takeda, Y., 1987, *A&A* **186** 200.
Shao, M., Colavita, M. M., Hines, B. E., Staelin, D. H., Hutter, D. J, 1988, *A&A*, **193**, 357.
Tuthill, P.G., 1994, PhD Dissertation, University of Cambridge.
Tsuji, T. 1978, *PASJ*, **30**, 435
van Belle, G. T., Dyck, H. M., Benson, J. A., Lacasse, M.G., 1996, *AJ*, **112**, 2147.
Walker, M.F., 1958, *ApJ*, **128**, 562.

Table 1. Primary calibration stars for the survey.

Name	HD	Spectral Type	Reference	Radius (R_{SUN})	Distance (pc)	Theta (mas)
γ Tri	14055	A1V	C+69	2.3±0.2	36.1±1.0	0.59±0.06
41 Ari	17573	B8V	GG94	3.0±0.3	49.0±1.9	0.57±0.06
υ Tau	28024	A8V	C+69	1.5±0.2	47.4±1.8	0.29±0.03
χ Her	142373	F8Ve	KM89	1.1±0.1	15.9±0.1	0.64±0.06
σ Cyg	202850	B9Iab	MWC53	38.0±11.4	1389±1119	0.25±0.22
51 Peg	217014	G5V	?	1.1±0.1	15.4±0.2	0.67±0.07

Table 2. Comparison of previously estimated or measured temperatures and angular sizes to those obtained with PTI.

Star	Method	T_{EFF} (K)	PTI T_{EFF} (K)	Size (mas)	PTI Size (mas)	Reference	Notes
HR 5681	IRFM	4840	5091 ± 263	2.699	2.55 ± 0.06	Blackwell et al. 1979	
HR 8684	IRFM	4964	5017 ± 425			Castelli et al. 1997	
HR 5429	IRFM	4298	4470 ± 228	3.825	3.67 ± 0.11	Blackwell & Lynas-Gray 1994	
HR 5681	IRFM	4801	5091 ± 263	2.769	2.55 ± 0.06	Blackwell & Lynas-Gray 1994	
HR 8684	Interferometry			4.9±0.4	2.54 ± 0.07	Hutter et al. 1989	
HR 1791	Interferometry			1.15±0.05	1.48 ± 0.18	Mozurkewich et al. 1991	Systematic errors might be larger than stated formal error
HR 2630	Occultation			<1.5	1.25 ± 0.45	Richichi et al. 1996	

Table 3. Normalized visibilities of stars observed at PTI. *JD* is the Julian date of the observation, *HA* is the hour angle, *B* is the projected baseline, an V_N^2 is the normalized visibility squared.

Name	*JD* (d)	*HA* (hr)	*B* (m)	V_N^2
BS 79	50737.77	-0.08	109.8	0.386±0.024
BS 157	50736.75	-0.72	109.6	0.722±0.048
BS 157	50736.77	-0.38	109.7	0.770±0.083
BS 157	50736.78	-0.05	109.8	0.849±0.093
BS 157	50736.79	0.17	109.8	0.797±0.061
BS 157	50736.80	0.37	109.8	0.795±0.057
BS 157	50736.82	0.80	109.7	0.794±0.072
BS 157	50736.83	1.21	109.6	0.741±0.077
BS 157	50736.84	1.45	109.6	0.744±0.071
BS 157	50736.85	1.65	109.5	0.729±0.064
BS 157	50737.73	-1.19	109.2	0.742±0.072
BS 157	50737.75	-0.69	109.6	0.757±0.046
BS 157	50737.76	-0.43	109.7	0.773±0.060
BS 157	50737.78	-0.03	109.8	0.769±0.066
BS 259	50737.79	-0.13	108.3	0.106±0.009
BS 274	50737.79	-0.09	109.3	0.307±0.041
BS 274	50737.78	-0.27	109.5	0.305±0.029
BS 274	50737.80	0.00	109.2	0.285±0.022
BS 351	50737.80	-0.04	106.9	0.665±0.054
BS 389	50737.81	-0.11	109.3	0.468±0.038
BS 450	50737.82	0.07	105.5	0.433±0.032
BS 564	50737.83	-0.13	109.1	0.248±0.016
BS 631	50737.84	-0.25	106.8	0.099±0.007
BS 631	50737.84	-0.17	106.6	0.107±0.008
BS 736	50737.85	-0.24	109.7	0.351±0.039
BS 882	50737.88	0.08	109.8	0.530±0.033
BS 1343	50737.90	-0.86	109.6	0.760±0.057
BS 1409	50737.92	-0.64	107.6	0.394±0.024
BS 1533	50737.93	-0.72	109.3	0.271±0.026
BS 1551	50737.93	-0.68	109.5	0.311±0.026
BS 1641	50728.01	0.38	109.5	0.771±0.105
BS 1641	50728.02	0.71	109.6	0.829±0.108

Name	*JD* (d)	*HA* (hr)	*B* (m)	V_N^2
BS 1641	50728.03	0.95	109.7	0.771±0.099
BS 1641	50728.04	0.98	109.7	0.799±0.099
BS 1641	50744.91	-0.87	108.3	0.770±0.065
BS 1641	50744.00	1.09	109.7	0.868±0.070
BS 1739	50737.95	-0.76	108.7	0.783±0.059
BS 1791	50737.96	-0.59	109.6	0.724±0.054
BS 1995	50737.00	0.01	109.6	0.571±0.039
BS 1995	50737.98	-0.42	109.3	0.607±0.054
BS 2012	50743.99	0.06	109.6	0.318±0.022
BS 2012	50744.95	-0.62	109.1	0.315±0.020
BS 2147	50737.04	0.60	109.5	0.709±0.091
BS 2147	50737.98	-0.84	108.1	0.749±0.056
BS 2147	50738.01	-0.09	109.1	0.806±0.089
BS 2147	50738.02	0.17	109.3	0.791±0.085
BS 2189	50738.01	0.00	109.7	0.270±0.031
BS 2219	50738.02	0.14	109.2	0.528±0.056
BS 2630	50728.02	-1.34	109.7	0.794±0.115
BS 2696	50738.04	-0.33	109.3	0.277±0.019
BS 2805	50738.03	-0.71	108.7	0.606±0.028
BS 5429	50621.77	2.17	108.3	0.095±0.003
BS 5510	50621.77	2.07	109.0	0.595±0.017
BS 5638	50621.78	1.88	106.8	0.840±0.023
BS 5681	50621.79	1.86	109.1	0.364±0.009
BS 5709	50621.79	1.88	108.1	0.920±0.024
BS 5745	50621.79	1.84	106.3	0.489±0.013
BS 6107	50621.84	1.98	109.2	0.110±0.003
BS 6107	50621.84	2.03	109.2	0.115±0.006
BS 6258	50621.83	1.41	108.3	0.500±0.024
BS 6258	50621.88	2.43	108.2	0.721±0.155
BS 6584	50621.90	2.16	108.6	0.747±0.178
BS 6584	50622.86	1.34	108.8	0.473±0.016
BS 6644	50692.69	1.67	106.6	0.766±0.033
BS 6644	50692.74	2.75	106.7	0.750±0.026
BS 6695	50621.91	2.08	109.7	0.237±0.014
BS 6695	50622.87	1.25	109.8	0.208±0.006
BS 7064	50691.71	1.03	107.5	0.679±0.067
BS 7064	50691.75	2.15	106.9	0.678±0.061
BS 7064	50692.69	0.84	107.7	0.636±0.022
BS 7064	50692.74	1.93	107.0	0.645±0.021
BS 7237	50621.93	1.58	108.8	0.479±0.018
BS 7237	50622.89	0.50	109.4	0.481±0.012
BS 7238	50621.94	1.68	108.5	0.434±0.017
BS 7238	50622.89	0.59	109.1	0.412±0.015
BS 7515	50690.73	0.65	109.8	0.841±0.071
BS 7515	50690.78	1.75	109.7	0.812±0.025
BS 7515	50691.72	0.32	109.8	0.827±0.068
BS 7515	50691.76	1.38	109.8	0.892±0.071
BS 7515	50692.71	0.26	109.8	0.833±0.023
BS 7515	50692.76	1.37	109.8	0.833±0.024
BS 7515	50690.73	0.65	109.8	0.841±0.071
BS 7515	50690.78	1.75	109.7	0.812±0.025
BS 7515	50691.72	0.32	109.8	0.827±0.068
BS 7515	50691.76	1.38	109.8	0.892±0.071

Name	*JD* (d)	*HA* (hr)	*B* (m)	V_N^2
BS 7515	50692.71	0.26	109.8	0.833±0.023
BS 7515	50692.76	1.37	109.8	0.833±0.024
BS 7515	50621.94	1.12	109.8	0.827±0.029
BS 7515	50622.90	0.09	109.8	0.827±0.014
BS 7520	50690.72	0.37	109.7	0.056±0.005
BS 7520	50691.70	-0.15	109.8	0.058±0.005
BS 7520	50691.71	0.17	109.8	0.058±0.005
BS 7520	50692.70	-0.02	109.8	0.054±0.002
BS 7759	50726.69	1.41	109.8	0.252±0.052
BS 7806	50622.92	0.05	109.7	0.327±0.009
BS 7834	50736.59	-0.44	109.7	0.770±0.056
BS 7847	50736.60	-0.38	109.6	0.834±0.072
BS 7942	50736.61	-0.28	109.7	0.458±0.064
BS 7966	50736.60	-0.57	107.4	0.481±0.045
BS 7966	50736.62	-0.20	108.0	0.463±0.039
BS 7995	50690.75	-0.06	108.9	0.778±0.055
BS 7995	50690.80	1.26	107.4	0.798±0.022
BS 7995	50691.74	-0.23	109.1	0.841±0.056
BS 7995	50691.85	2.50	107.1	0.843±0.063
BS 7995	50692.72	-0.62	109.4	0.809±0.022
BS 7995	50692.78	0.77	107.9	0.801±0.029
BS 7995	50736.63	0.01	108.8	0.681±0.056
BS 8008	50622.94	-0.14	109.2	0.402±0.014
BS 8044	50736.64	0.06	106.0	0.189±0.015
BS 8306	50736.64	-0.56	108.7	0.185±0.017
BS 8306	50737.68	0.37	109.5	0.207±0.026
BS 8485	50690.82	0.17	109.6	0.276±0.009
BS 8485	50691.87	1.42	109.8	0.302±0.023
BS 8485	50692.79	-0.31	109.3	0.276±0.010
BS 8517	50690.84	0.54	108.1	0.196±0.007
BS 8517	50691.87	1.48	107.2	0.225±0.022
BS 8517	50692.79	-0.33	109.1	0.188±0.007
BS 8517	50692.85	0.92	107.6	0.207±0.015
BS 8555	50691.87	1.24	109.0	0.756±0.064
BS 8555	50692.73	-2.05	108.5	0.725±0.022
BS 8555	50692.79	-0.67	109.8	0.709±0.026
BS 8555	50690.81	-0.19	109.7	0.719±0.022
BS 8555	50691.87	1.24	109.0	0.756±0.064
BS 8555	50692.73	-2.05	108.5	0.725±0.022
BS 8555	50692.79	-0.67	109.8	0.709±0.026
BS 8684	50736.66	-1.27	109.7	0.356±0.021
BS 8684	50736.69	-0.42	108.8	0.374±0.016
BS 8684	50737.69	-0.38	108.7	0.384±0.033
BS 8830	50736.73	0.22	107.1	0.854±0.073
BS 8830	50736.75	0.59	107.6	0.796±0.069
BS 8830	50737.73	0.12	107.0	0.798±0.083
BS 8830	50737.75	0.63	107.6	0.751±0.064
BS 8830	50741.83	2.88	108.1	0.974±0.072
BS 8882	50690.84	-0.34	109.6	0.468±0.017
BS 8882	50691.82	-0.75	109.8	0.501±0.057
BS 8882	50691.88	0.68	108.9	0.507±0.052
BS 8882	50692.80	-1.13	109.8	0.461±0.027
BS 8882	50692.85	0.11	109.3	0.488±0.041

Name	*JD* (d)	*HA* (hr)	*B* (m)	V_N^2
BS 8930	50736.70	-1.01	108.6	0.662±0.038
BS 8930	50737.70	-0.97	108.6	0.657±0.066
BS 8930	50737.74	0.00	109.6	0.662±0.075
BS 8942	50736.66	-1.82	109.8	0.086±0.005
BS 8942	50736.71	-0.79	108.4	0.100±0.005
BS 8942	50737.71	-0.69	108.2	0.109±0.007
BS 8942	50737.74	0.05	106.7	0.108±0.008
BS 8953	50736.67	-1.67	109.8	0.376±0.018
BS 8953	50736.71	-0.70	109.1	0.384±0.022
BS 8953	50737.71	-0.61	109.0	0.391±0.028
BS 9035	50736.68	-1.85	109.8	0.386±0.023
BS 9035	50736.72	-0.78	108.6	0.430±0.019
BS 9035	50737.72	-0.69	108.5	0.431±0.033
BS 9055	50736.74	-0.41	108.2	0.431±0.029
BS 9055	50737.76	0.07	107.3	0.437±0.037
IRC+20092	50737.92	-0.86	108.9	0.437±0.032
IRC+30086	50737.90	-0.84	109.8	0.427±0.026
IRC+30105	50737.94	-0.72	109.8	0.287±0.019
IRC+30115	50743.96	-0.18	109.5	0.237±0.019
IRC+30115	50744.93	-0.80	109.8	0.220±0.018
IRC+30134	50736.94	-1.75	109.6	0.682±0.044
IRC+30134	50736.98	-0.75	109.7	0.702±0.033
IRC+30134	50736.99	-0.35	109.4	0.662±0.034
IRC+30134	50737.02	0.38	108.7	0.656±0.079
IRC+30134	50737.03	0.63	108.4	0.701±0.089
IRC+30134	50737.94	-1.62	109.7	0.682±0.036
IRC+30134	50737.95	-1.24	109.8	0.692±0.037
IRC+30134	50737.97	-0.80	109.7	0.701±0.037
IRC+30134	50737.99	-0.38	109.4	0.671±0.046
IRC+30134	50738.00	-0.06	109.1	0.681±0.062
IRC+30134	50743.95	-0.85	109.7	0.606±0.054
IRC+30134	50743.97	-0.49	109.5	0.618±0.052
IRC+30134	50743.99	0.06	109.0	0.607±0.052
IRC+30134	50744.02	0.82	108.2	0.592±0.054
IRC+30134	50744.93	-1.46	109.8	0.596±0.050
IRC+30134	50744.95	-0.97	109.8	0.579±0.048
IRC+30134	50744.96	-0.63	109.6	0.577±0.048
IRC+30293	50692.68	2.71	107.3	0.540±0.024
IRC+30309	50621.89	2.11	107.3	0.428±0.103
IRC+30309	50622.86	1.30	107.6	0.256±0.011
IRC+30412	50622.93	0.49	107.8	0.278±0.007
IRC+30415	50693.73	0.44	108.0	0.253±0.006
IRC+30415	50697.73	0.50	107.9	0.239±0.011

Name	*JD* (d)	*HA* (hr)	*B* (m)	V_N^2
IRC+30415	50697.75	1.13	107.2	0.241±0.008
IRC+30415	50697.77	1.64	106.9	0.242±0.008
IRC+30415	50697.79	2.15	106.7	0.240±0.008
IRC+30415	50698.74	0.89	107.5	0.237±0.016
IRC+30415	50698.76	1.44	107.0	0.248±0.009
IRC+30415	50698.78	1.98	106.7	0.250±0.008
IRC+30438	50736.61	-0.22	109.3	0.393±0.058
IRC+30465	50622.94	-0.15	109.7	0.472±0.026
IRC+30468	50622.94	-0.12	109.0	0.498±0.027
IRC+30486	50690.81	0.06	109.6	0.395±0.012
IRC+30486	50691.86	1.39	109.0	0.426±0.031
IRC+30486	50692.73	-1.81	108.9	0.400±0.015
IRC+30486	50692.78	-0.43	109.8	0.383±0.013
IRC+30493	50690.81	-0.19	109.7	0.719±0.022
IRC+30508	50690.82	-0.82	109.8	0.771±0.025
IRC+30508	50690.83	-0.53	109.7	0.772±0.028
IRC+30508	50691.82	-0.82	109.8	0.803±0.095
IRC+30508	50691.88	0.60	108.9	0.804±0.083
IRC+30508	50692.80	-1.21	109.8	0.755±0.040
IRC+30508	50692.85	0.04	109.4	0.783±0.063
IRC+40018	50737.80	-0.01	109.6	0.406±0.040
IRC+40022	50737.82	-0.01	109.8	0.376±0.026
IRC+40337	50690.73	1.11	109.8	0.776±0.079
IRC+40337	50690.77	2.20	109.8	0.748±0.034
IRC+40337	50691.70	0.59	109.7	0.839±0.079
IRC+40337	50691.75	1.71	109.8	0.851±0.068
IRC+40337	50692.70	0.72	109.7	0.798±0.025
IRC+40337	50692.75	1.88	109.8	0.782±0.024
IRC+40337	50690.73	1.11	109.8	0.776±0.079
IRC+40337	50690.77	2.20	109.8	0.748±0.034
IRC+40337	50691.70	0.59	109.7	0.839±0.079
IRC+40337	50691.75	1.71	109.8	0.851±0.068
IRC+40337	50692.70	0.72	109.7	0.798±0.025
IRC+40337	50692.75	1.88	109.8	0.782±0.024
IRC+40337	50621.93	1.49	109.8	0.789±0.032
IRC+40337	50622.88	0.42	109.6	0.320±0.037
IRC+40370	50690.79	1.71	109.7	0.554±0.017
IRC+40370	50691.77	1.23	109.7	0.615±0.048
IRC+40370	50692.77	1.32	109.7	0.540±0.032
IRC+50262	50692.68	2.02	109.3	0.712±0.031
IRC+50262	50692.68	2.02	109.3	0.712±0.031
IRC+50262	50621.88	2.18	109.3	0.709±0.139

Table 4. Uniform disk angular sizes

Name	V_N^2	θ_{UD} (mas)
BS 79	0.386±0.030	2.46±0.09
BS 157	0.763±0.025	1.35±0.08
BS 259	0.106±0.020	3.61±0.11
BS 274	0.294±0.024	2.77±0.08
BS 351	0.665±0.057	1.70±0.18
BS 389	0.468±0.042	2.23±0.12
BS 450	0.433±0.037	2.42±0.11
BS 564	0.248±0.024	2.94±0.09
BS 631	0.102±0.019	3.69±0.11
BS 736	0.351±0.043	2.57±0.13
BS 882	0.530±0.038	2.04±0.11
BS 1343	0.760±0.060	1.37±0.20
BS 1409	0.394±0.030	2.49±0.09
BS 1533	0.271±0.032	2.85±0.11
BS 1551	0.311±0.032	2.71±0.10
BS 1641	0.804±0.039	1.22±0.14
BS 1739	0.783±0.061	1.30±0.22
BS 1791	0.724±0.057	1.48±0.18
BS 1995	0.583±0.036	1.90±0.11
BS 2012	0.317±0.023	2.70±0.08
BS 2147	0.761±0.042	1.37±0.14
BS 2189	0.270±0.036	2.84±0.12
BS 2219	0.528±0.058	2.06±0.17
BS 2630	0.794±0.116	1.25±0.45
BS 2696	0.277±0.026	2.83±0.09
BS 2805	0.606±0.033	1.84±0.10
BS 5429	0.095±0.018	3.67±0.11
BS 5510	0.595±0.025	1.87±0.07
BS 5638	0.840±0.029	1.12±0.11
BS 5681	0.364±0.020	2.55±0.06
BS 5709	0.920±0.030	0.77±0.16
BS 5745	0.489±0.022	2.23±0.07
BS 6107	0.111±0.018	3.55±0.10
BS 6258	0.505±0.029	2.14±0.09
BS 6584	0.476±0.024	2.22±0.07
BS 6644	0.757±0.027	1.41±0.09
BS 6695	0.212±0.019	3.06±0.07
BS 7064	0.644±0.023	1.76±0.07
BS 7237	0.480±0.021	2.19±0.06
BS 7238	0.421±0.021	2.37±0.06
BS 7515	0.829±0.020	1.13±0.07
BS 7520	0.055±0.018	3.92±0.15
BS 7759	0.252±0.055	2.91±0.19
BS 7806	0.327±0.020	2.65±0.07
BS 7834	0.770±0.058	1.33±0.20
BS 7847	0.834±0.075	1.12±0.30
BS 7942	0.458±0.067	2.25±0.19
BS 7966	0.471±0.035	2.25±0.10
BS 7995	0.799±0.022	1.25±0.08
BS 8008	0.402±0.023	2.43±0.07
BS 8044	0.189±0.024	3.26±0.10
BS 8306	0.192±0.023	3.15±0.09
BS 8485	0.278±0.019	2.82±0.06
BS 8517	0.195±0.019	3.19±0.08
BS 8555	0.720±0.021	1.49±0.06
BS 8684	0.369±0.022	2.54±0.07
BS 8830	0.831±0.037	1.14±0.14
BS 8882	0.472±0.022	2.22±0.06
BS 8930	0.661±0.035	1.67±0.10
BS 8942	0.098±0.018	3.71±0.11
BS 8953	0.381±0.022	2.49±0.07
BS 9035	0.416±0.022	2.40±0.07
BS 9055	0.433±0.029	2.37±0.09
IRC+20092	0.437±0.037	2.33±0.11
IRC+30086	0.427±0.031	2.34±0.09
IRC+30105	0.287±0.026	2.78±0.09
IRC+30115	0.228±0.022	3.00±0.08
IRC+30134	0.656±0.021	1.68±0.06
IRC+30293	0.540±0.030	2.06±0.09
IRC+30309	0.258±0.021	2.94±0.08
IRC+30412	0.278±0.019	2.87±0.07
IRC+30415	0.246±0.018	3.01±0.07
IRC+30438	0.393±0.061	2.45±0.18
IRC+30465	0.472±0.032	2.21±0.09
IRC+30468	0.498±0.032	2.15±0.09
IRC+30486	0.394±0.019	2.44±0.06
IRC+30493	0.719±0.028	1.49±0.09
IRC+30508	0.772±0.024	1.33±0.08
IRC+40018	0.406±0.044	2.41±0.13
IRC+40022	0.376±0.032	2.49±0.10
IRC+40337	0.756±0.020	1.38±0.07
IRC+40370	0.557±0.023	1.96±0.07
IRC+50262	0.712±0.028	1.52±0.09

Table 5. Spectral Type, Photometry: V, V-K, K-[12]

Name	Other names	HD	Sptype	Sptype (BSC5)	Ref	V	V-K	K-[12]
BS 79		1632	K5III	K5III	HO87?	5.79	3.99	0.56
BS 157		3421	G2 Ib-II	G2.5IIa	KM89	5.48		
BS 259		5316	M4III	M4IIIab	E92, E67, HO87?	6.20	5.19	0.56
BS 274	68 Psc	5575	G6III	gG6	M90?	5.42	2.49	0.35
BS 351	84 Psc, Chi Psc	7087	G8.5III	G8.5III-IIIa	KM89	4.66	2.30	0.47
BS 389	91 Psc	8126	K5III	gK5	M90?	5.23	3.30	0.45
BS 450		9640	M2III	M2IIIab	E92	5.89	4.04	0.55
BS 564		11928	M2III	M2III	E92	5.82	4.39	0.55
BS 631	15 Ari	13325	M3III	M3IIIab	E92	5.75	4.86	0.61
BS 736	14 Tri	15656	K5III	K5III	R52, GR60?	5.15	3.49	0.57
BS 882	24 Per	18449	K2III	K2III	R52, GR60?	4.94	2.85	0.51
BS 1343	54 Per	27348	G8III	G8III	KM89	4.93	2.17	
BS 1409	74 Tau, Eps Tau	28305	G9.5III	G9.5IIICN0.5	KM89	3.55	2.20	0.50
BS 1533		30504	K3.5III	K3.5IIIBa0.2:	KM89	4.87	3.41	0.57
BS 1551	2 Aur	30834	K2.5III	K2.5IIIbBa0.4	KM89	4.77	3.29	0.63
BS 1641	eta Aur	32630	B3V	B3V	MK73	3.20	-0.51	
BS 1739	109 Tau	34559	G8III	G8III	M90?	4.88	1.99	0.54
BS 1791	112 Tau, Bet Tau	35497	B7III	B7III	C72	1.64	-0.41	
BS 1995	29 Aur, Tau Aur	38656	G8III	G8IIIFe-1	KM89	4.53	2.19	
BS 2012	32 Aur, Nu Aur	39003	K0III	G9.5III*	KM89	3.97	2.46	0.55
BS 2147		41467	K0III	K0III	H55	6.12		
BS 2189		42471	M2III	M2IIIa	E92	5.78	4.31	0.57
BS 2219	44 Aur, Kap Aur	43039	G9III	G8.5IIIb	KM89	4.35	2.41	0.62
BS 2630	42 Gem, Ome Gem	52497	G5I	G5IIa-Ib	KM76	5.18	2.19	0.39
BS 2696	63 Aur	54716	K3.5III	K4III-IIIa	KM89	4.89	3.38	0.50
BS 2805	66 Aur	57669	K1 IIIa Fe 1	K1+IIIaCN1	KM89	5.19	2.70	0.54
BS 5429	25 Boo, Rho Boo	127665	K3III	K3-III	KM89	3.57	2.91	0.56
BS 5510		130084	M1III	M1IIIb	E92	6.28	4.25	0.47
BS 5638	46 Boo	134320	K2III	gK2	SK90?	5.67	3.00	0.49
BS 5681	49 Boo, Del Boo	135722	G8III	G8IIIFe-1	KM89	3.50	2.28	0.49
BS 5709	omi CrB	136512	K0III	K0III	GR60	5.51	2.38	0.51
BS 5745		137853	M1III	gM1	E92	6.02	4.20	0.50
BS 6107	20 1CrB, Nu1 CrB	147749	M2III	M2IIIab	E67?	5.20	4.35	0.54
BS 6258	50 Her	152173	M1III	M1IIIa	E92	5.72	3.98	0.55
BS 6584		160677	M2III	M2IIIab	E92	6.03	4.20	0.55
BS 6644	87 Her, IRC+30316	162211	K0 IIIb	K2III	KM89, GR60	5.12	2.66	0.49
BS 6695	91 Her, the Her	163770	K1II	K1IIaCN+2	KM89	3.87	2.84	0.56
BS 7064		173780	K2III	K3III	KM89	4.84	2.83	0.39
BS 7237		177808	M0III	M0III	E67?	5.54	3.71	0.45
BS 7238		177809	M2.5III	M2.5IIIab	E92	6.06	4.33	0.49
BS 7515	15 Cyg, IRC+40361	186675	G8III	G7+III	KM89	4.90	2.17	0.47
BS 7520		186702	M1III	M1III	E92	6.40	5.62	0.57
BS 7759		193092	K3 IIIa Fe -1	K3.5IIab-IIb	KM89	5.24	3.79	0.46
BS 7806	39 Cyg	194317	K2.5III	K2.5IIIFe-0.5	KM89	4.44	3.00	0.58
BS 7834	41 Cyg	195295	F5II	F5II	MR50	4.02	1.05	0.54
BS 7847	44 Cyg	195593	F5I	F5Iab	MR50, B57	6.17	2.63	
BS 7942	52 Cyg	197912	K0III	G9.5III	KM89	4.23	2.36	
BS 7966	IRC+50341	198237	K3III	K3III	F61	6.40	4.08	
BS 7995	31 Vul	198809	G7III	G7IIIFe-1	KM89	4.61	1.64	0.80
BS 8008	32 Vul	199169	K4III	K4III	R52, GR60?	4.99	3.37	0.48
BS 8044		200044	M3III	M3IIIab	E92	5.65	4.44	0.50

Name	Other names	HD	Sptype	Sptype (BSC5)	Ref	V	V-K	K-[12]
BS 8306		206749	M2III	M2IIIab	KM89	5.49	4.18	0.60
BS 8485		211073	K2.5III	K3III	KM89	4.49	3.18	0.60
BS 8517		212047	M4III	M4III	E92	6.47	5.18	0.58
BS 8555	IRC+30493	212988		K2	HO87?	5.98	3.36	0.56
BS 8684	48 Peg, Mu Peg	216131	G8III	G8+III	KM89	3.48	2.05	0.52
BS 8830	7 And	219080	F0V	F0V	E60	4.52	0.75	0.40
BS 8882	63 Peg	220088	M0III	M0III	E67, HO87?	5.59	3.70	0.50
BS 8930	14 And	221345	K0III	K0III	KK53	5.22	2.49	0.53
BS 8942		221662	M3III	M3III	E92	6.06	5.07	0.59
BS 8953		221905	M1III	M1III	E92	6.45	4.59	
BS 9035		223755	M2.5III	M2III	E92	6.11	4.10	0.63
BS 9055		224303	M2III	M2III	E92	6.15	4.19	0.58
IRC+20092		30354	M2III		M68	8.40	6.28	0.71
IRC+30086		27796	M3III		M68	7.80	5.67	0.70
IRC+30105		33463	M2III			6.38	4.79	0.60
IRC+30115		35601	M1.5I		KM89	7.35	5.61	0.92
IRC+30134		40441	K5III		F66	6.72	3.99	0.58
IRC+30293	V904 Her	150102	M2III		H56	6.98	4.82	0.55
IRC+30309	V959 Her	159968	M1III		E76	6.42	5.01	0.62
IRC+30412		190788	M3I		KM89	7.86	6.19	0.83
IRC+30415	W Vul	191652	M5III		N90	11.10	9.37	1.24
IRC+30438	FG Vul		M5II		W58	9.35	7.02	0.80
IRC+30465	V2142 Cyg	200043	M3III		MP50	7.20	5.11	0.68
IRC+30468		200546	M2III		H56	7.20	5.16	0.54
IRC+30486	PP Peg	210514	M4III		MP50	7.10	5.20	0.60
IRC+30508	V349 Peg	219654	M1III		H56	7.80	4.81	0.58
IRC+40018		6262	M3III		MP50	7.08	4.90	0.62
IRC+40022	YZ Tri	9500	M4III		MP50	7.00	5.13	0.51
IRC+40337		177697	K5?			7.76	4.90	0.38
IRC+40370		227069	M8III		NM49	8.88	6.32	1.02
IRC+50262		155816	K2?			6.80	4.06	0.62

Table 6. Bolometric Flux, Effective Temperature, Distance, Radius

Name	θ_R (mas)	F_{BOL} (10^{-8} erg cm^{-2} s^{-1})	T_{EFF} (K)	Distance (pc)	Radius (R_{SUN})
BS 79	2.51 ± 0.09	45.9 ± 3.9	3844 ± 107	200.0 ± 36.0	54.1 ± 9.9
BS 157	1.38 ± 0.08	31.3 ± 10.9	4714 ± 434	312.5 ± 78.1	46.4 ± 11.9
BS 259	3.69 ± 0.11	59.1 ± 3.6	3379 ± 73	178.6 ± 25.5	70.9 ± 10.4
BS 274	2.83 ± 0.08	32.8 ± 3.9	3329 ± 110	217.4 ± 33.1	66.2 ± 10.3
BS 351	1.74 ± 0.18	59.6 ± 10.8	4936 ± 344	135.1 ± 12.8	25.3 ± 3.6
BS 389	2.28 ± 0.12	48.3 ± 4.3	4088 ± 142	105.3 ± 8.9	25.8 ± 2.6
BS 450	2.47 ± 0.11	41.8 ± 3.8	3786 ± 122	181.8 ± 23.1	48.4 ± 6.5
BS 564	3.00 ± 0.09	52.2 ± 3.5	3631 ± 83	147.1 ± 17.3	47.6 ± 5.8
BS 631	3.77 ± 0.11	79.1 ± 5.7	3596 ± 84	204.1 ± 37.5	82.8 ± 15.4
BS 736	2.63 ± 0.13	60.8 ± 5.3	4033 ± 134	120.5 ± 11.6	34.1 ± 3.7
BS 882	2.08 ± 0.11	55.1 ± 8.8	4416 ± 213	107.5 ± 9.2	24.1 ± 2.4
BS 1343	1.40 ± 0.20	39.1 ± 5.9	4948 ± 406	69.4 ± 3.9	10.5 ± 1.6
BS 1409	2.54 ± 0.09	127.6 ± 21.5	4932 ± 226	47.6 ± 1.8	13.0 ± 0.7
BS 1533	2.91 ± 0.11	78.3 ± 7.3	4081 ± 124	161.3 ± 20.8	50.6 ± 6.8
BS 1551	2.77 ± 0.10	87.8 ± 14.5	4305 ± 194	172.4 ± 23.8	51.4 ± 7.3
BS 1641	1.25 ± 0.14	1025.4 ± 358.7	11864 ± 1241	67.1 ± 3.2	9.0 ± 1.1
BS 1739	1.33 ± 0.22	38.3 ± 8.8	5053 ± 517	63.3 ± 3.6	9.0 ± 1.6
BS 1791	1.51 ± 0.18	2593.5 ± 1139.0	13584 ± 1705	40.2 ± 1.5	6.5 ± 0.8
BS 1995	1.94 ± 0.11	58.8 ± 16.8	4652 ± 359	65.4 ± 3.4	13.7 ± 1.1
BS 2012	2.76 ± 0.08	105.9 ± 30.6	4521 ± 334	65.9 ± 3.8	19.6 ± 1.3
BS 2147	1.40 ± 0.14	24.3 ± 13.0	4393 ± 627	256.4 ± 52.6	38.6 ± 8.9
BS 2189	2.90 ± 0.12	70.5 ± 14.3	3982 ± 219		
BS 2219	2.11 ± 0.17	72.1 ± 13.3	4702 ± 290	51.8 ± 2.1	11.7 ± 1.1
BS 2630	1.28 ± 0.46	44.4 ± 29.5	5347 ± 1310		
BS 2696	2.89 ± 0.09	72.4 ± 6.2	4016 ± 107	142.9 ± 18.4	44.5 ± 5.9
BS 2805	1.88 ± 0.10	27.5 ± 17.4	3908 ± 628	222.2 ± 49.4	45.0 ± 10.3
BS 5429	3.75 ± 0.11	187.1 ± 36.4	4470 ± 228	45.7 ± 1.7	18.4 ± 0.9
BS 5510	1.91 ± 0.07	35.3 ± 3.4	4128 ± 127		
BS 5638	1.14 ± 0.11	29.2 ± 2.4	5085 ± 271	128.2 ± 13.1	15.8 ± 2.2
BS 5681	2.61 ± 0.06	151.9 ± 30.5	5091 ± 263	35.8 ± 0.8	10.1 ± 0.3
BS 5709	0.79 ± 0.16	9.9 ± 5.6	4682 ± 824	84.0 ± 4.9	7.1 ± 1.5
BS 5745	2.28 ± 0.07	42.2 ± 3.3	3951 ± 99	238.1 ± 45.4	58.4 ± 11.3
BS 6107	3.63 ± 0.10	90.4 ± 12.1	3790 ± 138	169.5 ± 17.2	66.2 ± 7.0
BS 6258	2.19 ± 0.09	52.4 ± 5.6	4258 ± 145	285.7 ± 57.1	67.2 ± 13.7
BS 6584	2.27 ± 0.07	39.8 ± 2.5	3902 ± 87	163.9 ± 16.1	40.0 ± 4.1
BS 6644	1.44 ± 0.09	41.6 ± 6.3	4953 ± 245	62.9 ± 2.4	9.8 ± 0.7
BS 6695	3.13 ± 0.07	160.8 ± 52.8	4714 ± 390	204.1 ± 20.8	68.7 ± 7.2
BS 7064	1.80 ± 0.07	55.9 ± 6.4	4773 ± 167	76.9 ± 3.0	14.9 ± 0.8
BS 7237	2.24 ± 0.06	47.2 ± 3.4	4102 ± 92	185.2 ± 20.6	44.6 ± 5.1
BS 7238	2.42 ± 0.06	42.6 ± 2.9	3843 ± 82	227.3 ± 31.0	59.2 ± 8.2
BS 7515	1.15 ± 0.07	41.8 ± 4.4	5540 ± 225	85.5 ± 3.7	10.6 ± 0.8
BS 7520	4.01 ± 0.15	64.4 ± 3.7	3313 ± 79	256.4 ± 39.4	110.6 ± 17.5
BS 7759	2.97 ± 0.19	74.7 ± 4.7	3991 ± 145	303.0 ± 45.9	97.0 ± 16.0
BS 7806	2.71 ± 0.07	92.2 ± 20.4	4408 ± 250	78.1 ± 3.7	22.8 ± 1.2
BS 7834	1.36 ± 0.20	95.5 ± 33.5	6277 ± 725	232.6 ± 27.0	34.0 ± 6.5
BS 7847	1.14 ± 0.31	22.3 ± 11.6	4757 ± 888		

Name	θ_R (mas)	F_{BOL} (10^{-8} erg cm^{-2} s^{-1})	T_{EFF} (K)	Distance (pc)	Radius (R_{SUN})
BS 7942	2.30 ± 0.19	84.2 ± 38.5	4677 ± 569	63.3 ± 2.4	15.7 ± 1.5
BS 7966	2.30 ± 0.10	34.9 ± 4.6	3751 ± 150	400.0 ± 96.0	99.0 ± 24.2
BS 7995	1.28 ± 0.08	51.2 ± 14.2	5539 ± 423	66.2 ± 2.6	9.1 ± 0.7
BS 8008	2.48 ± 0.07	70.6 ± 6.8	4306 ± 121	227.3 ± 36.2	60.7 ± 9.8
BS 8044	3.33 ± 0.10	63.1 ± 4.4	3615 ± 84	181.8 ± 26.4	65.2 ± 9.7
BS 8306	3.22 ± 0.09	66.7 ± 5.0	3729 ± 87	181.8 ± 19.8	63.0 ± 7.1
BS 8485	2.88 ± 0.06	103.5 ± 29.2	4398 ± 314	172.4 ± 17.8	53.5 ± 5.6
BS 8517	3.26 ± 0.08	50.4 ± 6.2	3454 ± 114	243.9 ± 47.6	85.6 ± 16.8
BS 8555	1.52 ± 0.06	31.9 ± 2.4	4507 ± 123	285.7 ± 57.1	46.8 ± 9.6
BS 8684	2.60 ± 0.07	142.1 ± 47.5	5017 ± 425	35.8 ± 1.0	10.0 ± 0.4
BS 8830	1.17 ± 0.14	39.9 ± 13.4	5452 ± 566	24.5 ± 0.4	3.1 ± 0.4
BS 8882	2.27 ± 0.06	43.6 ± 6.8	3994 ± 164	133.3 ± 12.4	32.6 ± 3.2
BS 8930	1.71 ± 0.10	33.3 ± 4.5	4305 ± 194	76.3 ± 4.1	14.0 ± 1.1
BS 8942	3.79 ± 0.11	71.7 ± 7.4	3498 ± 104		
BS 8953	2.54 ± 0.07	49.3 ± 28.0	3889 ± 554		
BS 9035	2.45 ± 0.07	36.3 ± 3.2	3668 ± 96	166.7 ± 22.2	44.0 ± 6.0
BS 9055	2.42 ± 0.09	36.5 ± 2.8	3696 ± 99	185.2 ± 27.4	48.3 ± 7.4
IRC+20092	2.38 ± 0.11	33.2 ± 5.3	3640 ± 169		
IRC+30086	2.39 ± 0.09	18.2 ± 1.1	3125 ± 76		
IRC+30105	2.84 ± 0.09	47.3 ± 6.1	3642 ± 131		
IRC+30115	3.07 ± 0.08	29.0 ± 2.4	3103 ± 76		
IRC+30134	1.72 ± 0.06	16.7 ± 0.5	3610 ± 70		
IRC+30293	2.11 ± 0.09	25.3 ± 2.4	3619 ± 116		
IRC+30309	3.00 ± 0.08	49.5 ± 4.1	3582 ± 89		
IRC+30412	2.93 ± 0.07	33.1 ± 3.7	3280 ± 99		
IRC+30415	3.08 ± 0.07	28.4 ± 2.1	3080 ± 67		
IRC+30438	2.50 ± 0.18	11.0 ± 1.2	2695 ± 123		
IRC+30465	2.26 ± 0.09	27.1 ± 1.5	3554 ± 88	294.1 ± 60.6	71.5 ± 15.0
IRC+30468	2.20 ± 0.09	25.1 ± 1.9	3535 ± 99	263.2 ± 55.4	62.2 ± 13.4
IRC+30486	2.49 ± 0.06	38.5 ± 7.8	3692 ± 191		
IRC+30508	1.52 ± 0.09	29.3 ± 14.9	4415 ± 576	1000.0 ± 800.0	163.9 ± 131.5
IRC+40018	1.36 ± 0.08	27.9 ± 4.6	4616 ± 234		
IRC+40022	2.46 ± 0.13	35.9 ± 6.7	3652 ± 197		
IRC+40337	2.54 ± 0.10	18.5 ± 5.0	3042 ± 213		
IRC+40370	1.41 ± 0.07	11.9 ± 0.3	3663 ± 95		
IRC+50262	2.00 ± 0.07	24.2 ± 2.5	3668 ± 114	400.0 ± 96.0	86.2 ± 20.9

Table 7. Effective temperature, linear radii as a function of spectral type: observed data and fits. Error bars are standard deviations by spectral type. N_T and N_R represent the number of data points for each spectral type bin for effective temperature and radius analyses, respectively. The mean standard deviation of T_{EFF} is 7% of the weighted average for each of the spectral type bins; the same number for R_{AVG} is 60% by spectral type. T_{FIT} and R_{FIT} are the results of weighted chi-squared minimizations to the temperature data for stars in spectral classes G7 through M8. $\chi^2(T_{FIT})=4.21$, $\chi^2(R_{FIT})=9.49$. The average standard deviation of T_{EFF} is 270 K and represents the accuracy of T_{FIT}; the corresponding number for R_{FIT} is the average standard deviation size of 60%.

Spectral Type	N_T	T_{EFF} (K)	T_{FIT} (K)	N_R	R_{AVG} (R_{SUN})	R_{FIT} (R_{SUN})
G7	1		4840	1		8.7
G8	7	5133 ± 286	4735	7	10.3 ± 6.3	10.1
G9	3	4864 ± 134	4630	3	13.0 ± 8.7	11.7
K0	8	4646 ± 231	4525	8	12.5 ± 10.6	13.8
K1	4	4264 ± 415	4420	3	23.8 ± 8.7	16.4
K2	8	4598 ± 267	4315	8	18.5 ± 18.6	19.5
K3	8	4072 ± 279	4210	8	21.5 ± 46.3	23.5
K4	4	4122 ± 127	4105	4	44.8 ± 10.0	28.4
K5	6	3851 ± 207	4001	5	40.1 ± 12.9	34.5
M0	7	3973 ± 265	3896	7	50.1 ± 22.1	42.1
M1	12	3768 ± 338	3791	7	63.3 ± 22.6	51.5
M2	17	3741 ± 150	3686	12	58.5 ± 24.4	63.2
M3	17	3623 ± 326	3581	14	71.8 ± 27.1	77.7
M4	15	3426 ± 417	3476	9	104.0 ± 25.0	95.7
M5	15	3366 ± 433	3371	9	139.6 ± 44.7	118.1
M6	6	3375 ± 106	3266	4	147.9 ± 41.1	145.8
M7	6	3095 ± 279	3162	3	131.9 ± 109.9	180.3
M8	1		3057	0		223.1

Table 8. Effective temperature, linear radii as a function of V-K color: observed data, fits, and temperature expectations for a black body radiator. Error bars are standard deviations by V-K bin. N_T and N_R represent the number of data points for each spectral type bin for effective temperature and radius analyses, respectively. The mean standard deviation of T_{EFF} is 7% of the weighted average for each of the V-K bins; the same number for R_{AVG} is 35% by V-K bin. T_{FIT} and R_{FIT} are the results of weighted chi-squared minimizations to the temperature data for stars with 1.5 < V-K < 9.0. $\chi^2(T_{FIT})$=2.74, $\chi^2(R_{FIT})$=9.88. All of the T_{EFF} values for V-K ≥ 6.0 deviate from T_{BBR} by 3σ or more. The average standard deviation of T_{EFF} is 260 K and represents the accuracy of T_{FIT}; the corresponding number for R_{FIT} is the average standard deviation size of 35%.

V-K Bin	Bin size	N_T	T_{EFF} (K)	T_{FIT} (K)	T_{BBR}	N_R	R_{AVG} (R_{SUN})	R_{FIT} (R_{SUN})
2.0	0.5	6	5106 ± 304	4900	4899	6	10.9 ± 1.8	7.9
2.5	0.5	12	4553 ± 389	4570	4343	12	11.1 ± 11.6	15.0
3.0	0.5	7	4615 ± 257	4297	3908	7	19.0 ± 14.6	23.2
3.5	0.5	11	4096 ± 114	4070	3558	11	37.9 ± 11.3	32.9
4.0	0.5	20	3816 ± 207	3883	3268	18	57.6 ± 19.4	44.2
4.5	0.5	13	3756 ± 227	3727	3025	10	69.1 ± 23.1	57.4
5.0	0.5	17	3565 ± 387	3599	2816	7	79.1 ± 15.1	72.8
5.5	0.5	12	3435 ± 463	3492	2636	9	118.0 ± 13.7	90.8
6.0	0.5	4	3566 ± 213	3404	2478	3	161.4 ± 17.2	111.9
6.5	0.5	3	3544 ± 152	3331	2339	0		136.5
7.0	0.5	6	3320 ± 359	3271	2215	3	166.8 ± 59.2	165.2
7.5	0.5	5	3364 ± 125	3221	2104	4	129.4 ± 47.5	198.7
8.0	1.0	4	3294 ± 136	3179	2003	3	190.3 ± 23.8	237.9
9.0	1.0	3	3000 ± 337	3117	1829	1		

Table 9. Effective temperature, linear radii as a function of K-[12] color: observed data, fits, and temperature expectations for a black body radiator. Error bars are standard deviations by K-[12] bin. N_T and N_R represent the number of data points for each spectral type bin for effective temperature and radius analyses, respectively. The mean standard deviation of T_{EFF} is 11% of the weighted average for each of the K-[12] bins; the same number for R_{AVG} is 200% by K-[12] bin. All of the T_{EFF} values for K-[12] ≥ 0.90 deviate from T_{BBR} by 2.5σ or more.

K-[12] Bin	Bin size	N_T	T_{EFF} (K)	T_{BBR} (K)	N_R	R_{AVG} (R_{SUN})
0.35	0.05	1		5454	1	
0.40	0.05	3	3929 ± 923	5076	2	15.2 ± 78.0
0.45	0.05	7	4225 ± 665	4741	6	13.3 ± 40.7
0.50	0.05	18	4039 ± 605	4453	17	11.3 ± 30.1
0.55	0.05	25	3708 ± 442	4205	22	20.6 ± 49.5
0.60	0.05	26	3645 ± 470	3981	19	24.2 ± 66.8
0.65	0.05	11	3752 ± 432	3784	11	33.0 ± 69.9
0.70	0.10	11	3580 ± 232	3608	6	93.0 ± 42.4
0.80	0.10	1		3304	1	
0.90	0.10	3	3536 ± 83	3052	2	108.0 ± 11.1
1.00	0.20	5	3457 ± 152	2839	3	144.7 ± 44.9
1.20	0.30	3	3255 ± 155	2499	1	
1.50	0.30	3	3250 ± 154	2130	2	202.2 ± 15.1
1.80	0.30	3	2959 ± 442	1865	1	

Figures 1a,b. Temperature, radius as a function of spectral type.

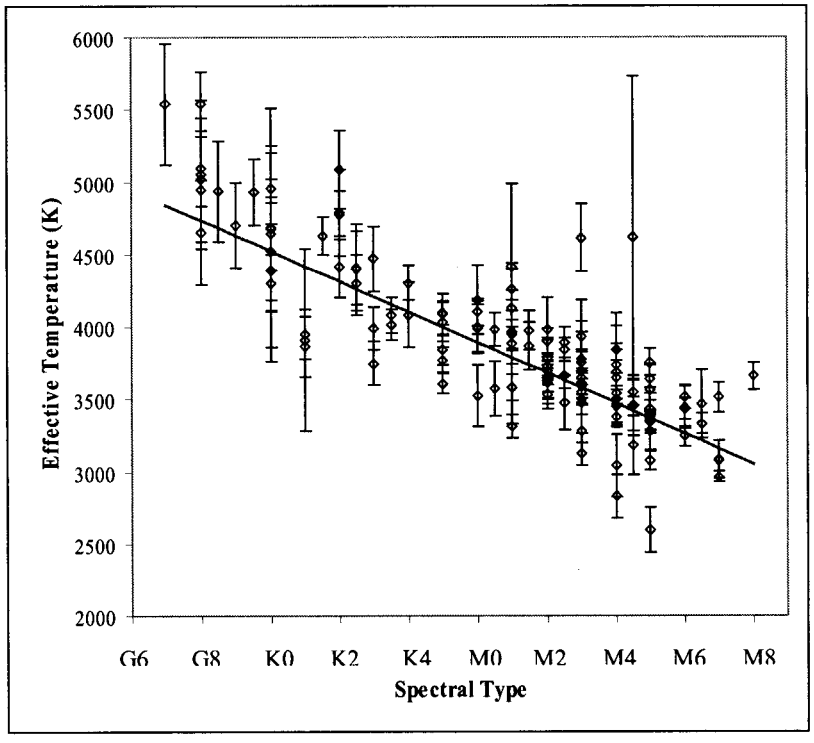

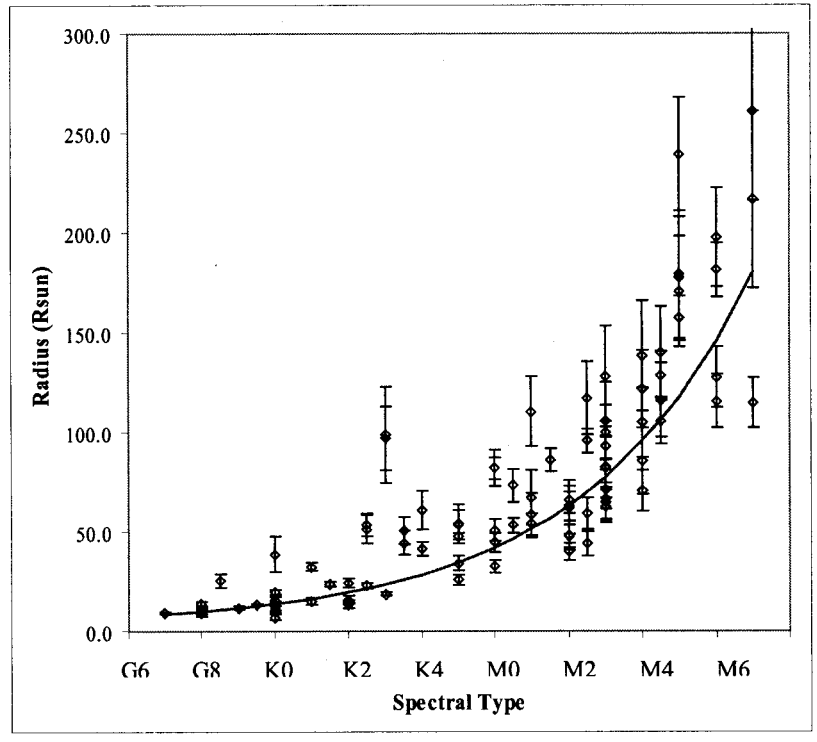

Figures 2a, b. Effective temperature and radius as a function of V-K color. The strong departure from blackbody behavior (the dotted line) at V-K $\geq$ 6.0 is indicated to be statistically significant by the data at the 3σ level.

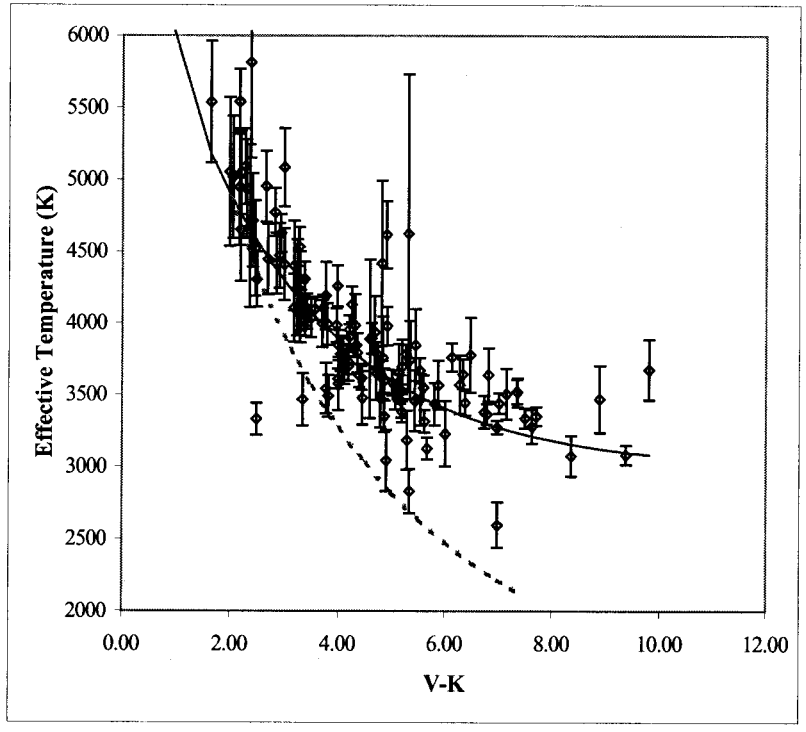

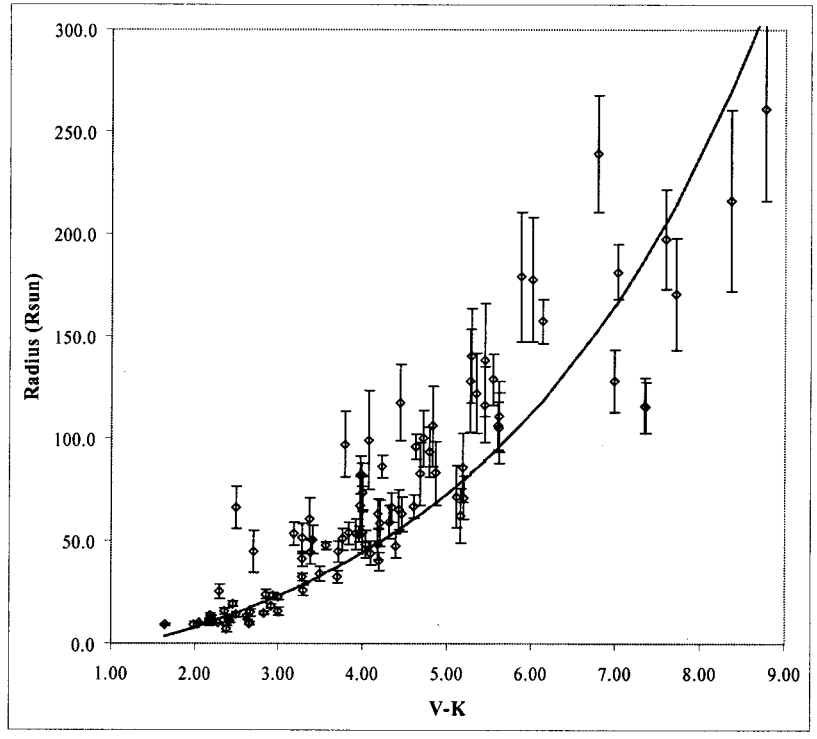

Figures 3a, b. Effective temperature and radius as a function of K-[12] color. Note the strong departure from blackbody behavior at K-[12] > 0.80; it is statistically signficant at the 2.5σ level.

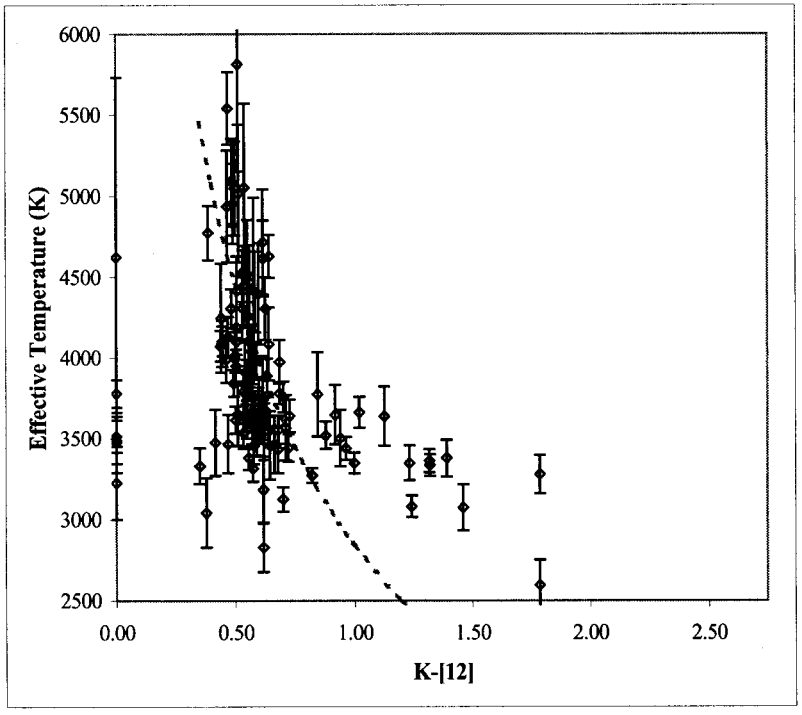

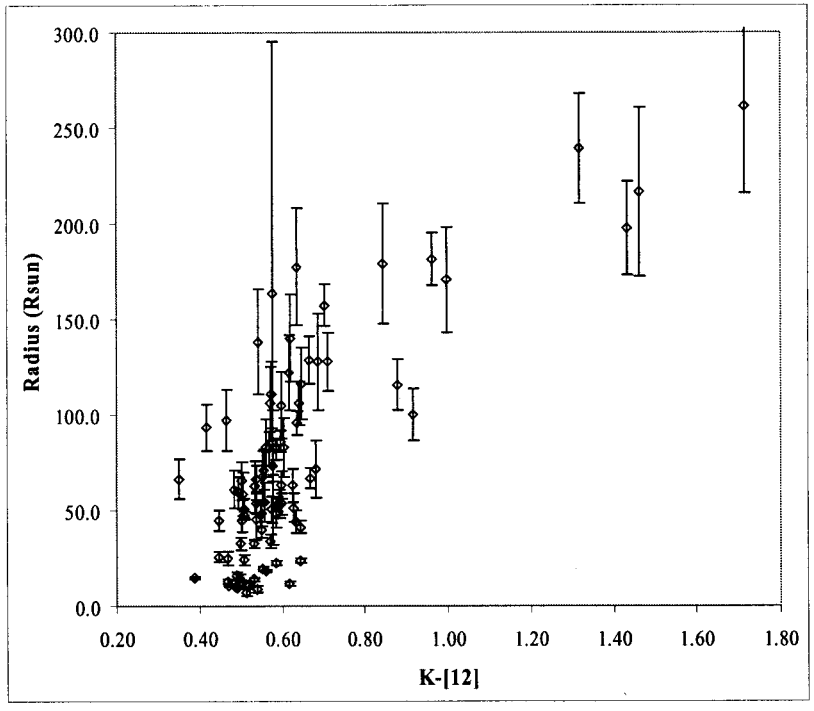

Figure 4. Radius as a function of effective temperature by luminosity class. Representative error bars are 4% for temperature and 18% for radius, from the data given in the paper. The luminosity class I and II objects are on average ~3 times the radius of the giant stars for a given temperature.